Optical properties of CdS nanocrystalline thin films in the abrupt phase transition from zinc blende to wurtzite

C. G. Torres-Castanedo[1] · J. Márquez-Marín[2] · R. Castanedo-Pérez[2] · G. Torres-Delgado[2] · M. A. Aguilar-Frutis[3] · S. Arias-Cerón[4] · O. Zelaya-Ángel[5]

Abstract

A set of cadmium sulfide (CdS) thin films was grown on glass substrates by the chemical bath deposition technique at different bath temperatures (T_b). A microwave oven was used to heat the precursor aqueous solution employed to prepare the films in the 60–97 °C interval. The average crystallite size of the CdS films lies in the 7–20 nm range, calculated from X-ray diffraction data. The diffraction patterns reveal that the crystalline structure of CdS nanoparticles is cubic zinc blende (ZB) for $60 \leq T_b \leq 93$ °C, hexagonal wurtzite (WZ) for $95 \leq T_b \leq 97$ °C, and ZB-WZ mix of phases for the critical temperature $T_b \cong 94$ °C (T_{bc}). The mixture of both phases is supported by Transmission Electron Microscopy. The CdS films show preferred orientation along (111) and (002) directions for ZB and WZ, respectively. The optical properties reveal significant changes at T_{bc}, namely, the energy band gap, photoluminescence emission, and refractive index. The photoluminescence results show an additional band at the critical phase transition temperature due to the presence of a high-density Cd interstitial/vacancies, produced by the mix of phases. Furthermore, high-energy transitions above the conduction band also exhibit splitting due to the phase transition.

1 Introduction

The II–VI compound semiconductors are widely studied due to their promising applications in nano-dimensional structures. Cadmium sulfide (CdS) is a semiconductor compound that was initially investigated as a fluorescent material for image reproduction [1, 2]. Nowadays, CdS is widely employed in solar cells, optoelectronic devices, lasers, gas sensors, biological, and pharmaceutic products [3–7].

Recently, Li et al. [8] published a review on the nanostructured cadmium sulfide as a promising semiconductor for profitable optoelectronic devices. According to this report, CdS nanocrystals can be utilized to prepare functional lasers, waveguides, photovoltaics, among others. There has been an increasing interest in nanostructured CdS due to a wide variety of industrial applications such as photocatalysis [9], photoelectrochemistry [10], as an antimicrobial [11], ferromagnetism [12], and medical imaging [13]. CdS has been synthesized in three different crystalline structures: cubic zinc blende (ZB), hexagonal wurtzite (WZ), and cubic rock salt (RS). As nanocrystals, WZ and ZB phases are stable at standard conditions, while RS is stable only at high pressures. However, recently, the WZ-to-RS transformation in nanocrystalline flower-shaped CdS at atmospheric pressure has been reported [14]. The direct band gap (E_g) of nanodimensional WZ and ZB phases can oscillate between 2.42 to 3.85 eV depending on the crystallite size and morphology [15]. Indirect E_g values of the RS structure are located between 0.8 and 1.7 eV in the pressure range $0 \leq P \leq 70$ GPa [16, 17]. The RS indirect E_g values are also dependent on the size of the nanoparticles (NP's) [18]. Due to the wide variety of CdS applications, the study of the properties associated

✉ O. Zelaya-Ángel
ozelaya@fis.cinvestav.mx

1 Depto. de Física, Centro de Investigación y de Estudios Avanzados del Instituto Politécnico Nacional, Mexico 07360, México

2 Unidad Querétaro, Centro de Investigación y de Estudios Avanzados del I.P.N., 76230 Querétaro, QRO, Mexico

3 Centro de Investigación en Ciencia Aplicada y Tecnología Avanzada del I.P.N., 11500 Mexico, Mexico

4 Depto. de Ingeniería Eléctrica, SEES, Centro de Investigación y de Estudios Avanzados del I.P.N., 07360 Mexico, Mexico

5 Facultad de Ingeniería, Universidad Autónoma de Querétaro, Centro Universitario, 76010 Querétaro, QRO, Mexico

with the different crystalline phases has become a fundamental task [3], especially in nanoparticles [19].

Stable ZB and WZ-CdS phases have been extensively used in different applications with no clear evidence of a preferred structure. For instance, ZB shows improved performance for water splitting in ZnO/CdS nanocomposites [20], while WZ does the same for the CdS/Cd(OH)$_2$ nanostructure [21]. In the case of photoluminescence (PL), some authors have obtained an enhancement in PL using WZ [22] and others with ZB [23]. Gaiardo et al. reported that ZB-CdS nanoparticles are ideal for chemoresistive gas sensors [24], and Li et al. found that WZ-CdS nanoparticles are excellent candidates for detectors in photoelectrochemical sensing of gases [25]. Also, some authors have reported that WZ, ZB, and WZ+ZB phases are suitable materials for devices such as LEDs [26], solar cells [27], photocatalysts [28], etc. With respect to the ZB$\leftrightarrow$WZ phase transformation, the disorder generated by the phase change can produce non-expected behaviors, especially in CdS or CdSe, due to the low energy of transition (~ 2 meV) [29]. This fact indicates that special care must be considered when planning an experiment since some perturbation could trigger a phase transformation.

Nanocrystalline CdS thin films have been synthesized by different techniques such as chemical bath deposition (CBD) [30], spray pyrolysis [31], precipitation [32], thermal evaporation [33], vapor sublimation [34], etc. In this work, we report the optical properties during the ZB to the WZ phase transition of CdS-nanoparticulated thin films grown by CBD. The samples were grown at different temperatures in the 60 to 97 °C interval, using a microwave oven to heat the growth solution. The phase transition occurs in the bath temperature (T_b) 93–95 °C range, which is an abrupt change of structure. Band gap, refractive index, and photoluminescence effects from the ZB-to-WZ transformation are discussed. A blue shift is observed in the band gap, expected for spherical NP´s in the intermediate quantum confinement (IQC) [35, 36].

2 Experimental details

The aqueous solutions were prepared by using ~ 625 ml of ultrapure deionized water. All the reagents employed were high purity: (a) Cd(CH$_3$COO)$_2$·2H$_2$O, 1.372×10^{-3} mol, 243.2 mg, (b) CH$_3$CO$_2$NH$_4$, 27.56×10^{-3} mol, 1413 mg, (c) NH$_4$OH, 28–30%, 30 ml, and (d) NH$_2$CSNH$_2$, 6.124×10^{-3} mol, 310 mg. Glass substrates Corning 2947 were ultrasonically cleaned in a residue-free detergent solution and subsequently immersed in a chromic acid solution for 24 h. Then they were placed in an aqueous nitric acid solution (1:3) at 75 °C for 3 h and rinsed in deionized water. Finally, the substrates were dried with N$_2$. The growing reactor was a commercial microwave oven, and the temperature

was regulated using an N1100 Novus controller. The samples were deposited at different bath temperatures (T_b): 60, 70, 80, and 90 °C and for T_b's between 90 and 97 °C with 1 °C steps. For each T_b, the temperature was automatically controlled within ± 0.2 °C [30]. This control is achieved since the microwaves heat up uniformly and rapidly all the volume of the aqueous solution, which is continuously stirring. The deposition time was varied from ½ h for the film deposited at 97 °C, up to 24 h for $T_b = 60$ °C, to obtain similar thicknesses for the samples (200–250 nm). X-ray diffraction (XRD) patterns were obtained using a Rigaku D/max-2100 diffractometer (CuKα radiation, 0.15406 nm), equipped with a thin film attachment. The thickness was measured by utilizing a Dektak II profilometer. Surface morphology was observed by a scanning electron microscope (SEM) Philips XL30-ESE. Transmission electron microscopy (TEM) images were obtained in a Jeol 2010 microscope working at 200 keV; small pieces of the CdS films were detached from the substrate and put onto the TEM grid. Selected area electron diffraction (SAED) patterns were analyzed with the Diamond 3.0 software. Photoluminescence measurements were performed by a 0.5 m spectrometer (Jovin-Ivon) equipped with a 325 nm line of a He–Cd laser. An ellipsometer (Jobin-Ivon Uvisel) was used for the measurements in the 1.5 to 4.5 eV interval. The ellipsometry results were compared with the theoretically calculated spectra using the software available in the ellipsometer (Psi-Delta 2.0). All the experimental characterization was performed at room temperature (RT).

3 Results and discussion

Figure 1 displays the XRD patterns in the range $20 \leq 2\theta \leq 60$ degrees for the set of eleven films. According to the XRD data, the CdS nanoparticles (NP's) in the films grow with cubic symmetry for $60 \leq T_b < 94$ °C, and a hexagonal symmetry for $94 < T_b \leq 97$ °C. At the critical temperature ($T_{bc} = 94$ °C), the films grow with a mix of both crystalline phases. The (002) is the preferential orientation of the films for WZ and the (111) for ZB is observed in diffractograms. In the hexagonal structure, small zones grow with cubic symmetry and vice versa, whose proportion depends on the closeness to T_{bc}. Figure 1 shows that the XRD intensity increases with T_b, showing an increase of crystallinity with temperature in both ZB and WZ phases.

In Fig. 2 (I), a 36 nm × 42 nm TEM image shows the NP dimensions of the crystallites in the film grown at 94 °C, where both ZB and WZ phases of CdS coexist. The inset (a) displays the SAED pattern of this film, where the presence of both ZB and WZ crystalline phases are revealed by the diffracted rings, as noted in insets (b) and (c), respectively. The nanocrystals observed in Fig. 2(I) show the (111) and the (002) interplanar spacings of the ZB and the WZ
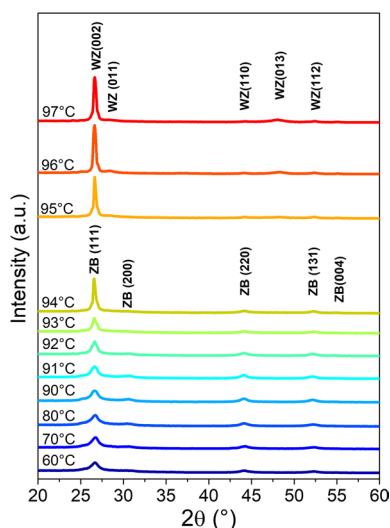
Fig. 1 XRD patterns in the $20 \leq 2\theta \leq 60$ degrees of all the CdS samples analyzed

Fig. 3 Direct band gap energy (Left) and average crystal size (Right) as a function of T_b

phases, respectively, which support the preferential orientation observed in XRD. In Fig. 2 (II), a SEM image shows the surface morphology of the film grown at $T_b = 94$ °C, which illustrates a homogeneous film with few isolated particles (average diameter ~ 200 nm) on the top. The more probable stacking on the amorphous substrate is (002) and (111) planes for WZ and ZB crystalline structures, respectively, since the difference of stacking energy is only 8 meV/atom [37].

CdS NP's average crystal size (ACS) as a function of T_b, obtained from the full width at half maximum (FWHM) of the XRD reflections, and calculated by the Scherrer equation, is displayed, the error bar of T_b is ± 0.2 °C in Fig. 3 (right). ACS is approximately constant (~ 6 nm) for $T_b < 91$ °C and increases abruptly after this temperature up to ~ 20 nm. The direct band gap energy (E_g) of the films (Fig. 3 left) was determined by optical absorbance spectra and calculated
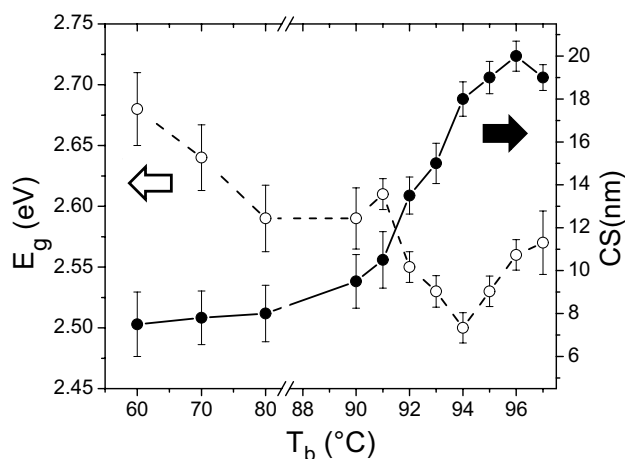
using the Tauc's formula (not shown here). An abrupt decrease of E_g is observed for 91 °C < T_b < 94 °C (T_{bc}), which corresponds to the increase of the ACS. E_g shows a minimum during the phase transition at $T_{bc} = 94$ °C. This behavior has been observed previously for the solid–solid ZB → WZ transformation of CdS and is explained by the fact that the CdS lattice has the maximum disorder at this point [38, 39]. In these reports, ZB-CdS was transformed to WZ-CdS through thermal annealing in an $Ar + S_2$ atmosphere in the temperature range of 60–550 °C. The gradual transformation occurs within an interval of ~ 100 °C, where T_{bc} was found to be at 300 °C. In the present case, almost all the ZB → WZ transition occurs in the T_b range 93–95 °C ($15.0 \leq ACS \leq 19$ nm), which is within ~ 0.2 meV. The phase transformation occurs very abruptly since it is not a solid–solid transformation. At least four factors are involved in the variation of E_g as a function of the T_b: disorder [40], strain [32], lattice structure [41], and intermediate quantum

Fig. 2 TEM image of the CdS sample prepared at $T_{bc} = 94$ °C (I). The coexistence of both ZB and WZ phases can be observed. The electron diffraction pattern of this sample is displayed in the inset (**a**). Insets (**b**, **c**) reveal that the sample has both WZ and ZB crystalline phases. SEM image of this sample surface (II)
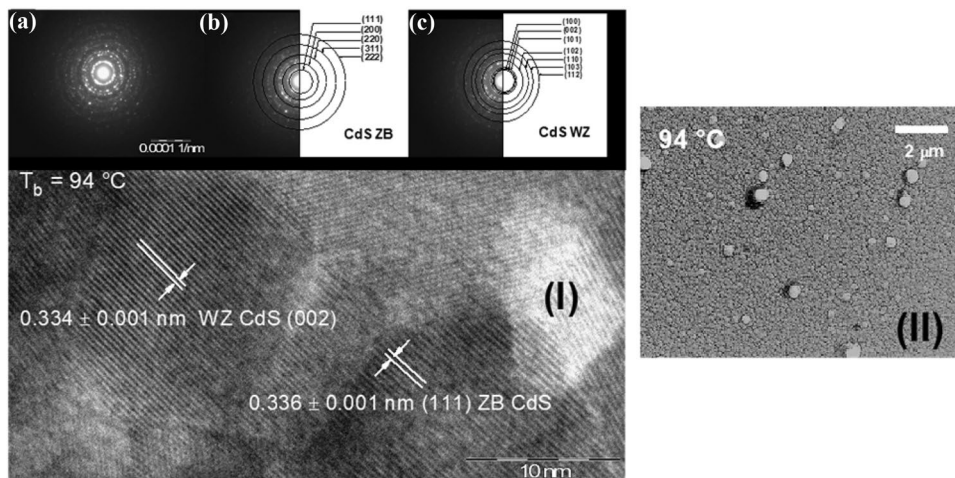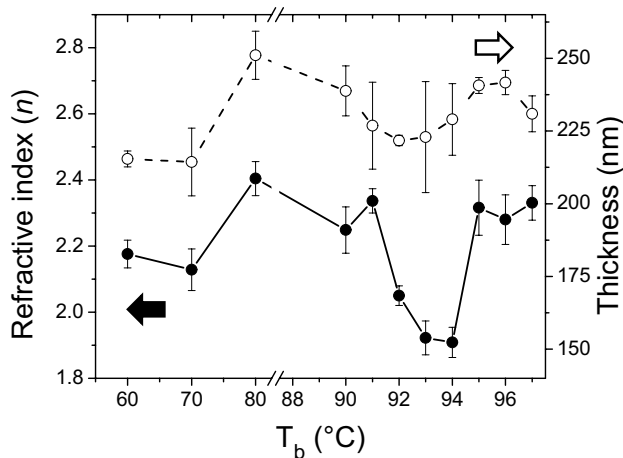
Fig. 4 Refractive index (n) (Left) and thickness (Right) vs. T_b for all the studied CdS thin films

confinement [42, 43]. IQC has been extended up to ACS of CdS NP's reported in this work because of the non-stoichiometry character of the films. CdS thin films prepared by CBD has an excess of Cd [44], which increases the E_g [45, 46].

The refractive index (n) was calculated from ellipsometry measurements (Fig. 4). Close to T_{bc}, the n values suffer a pronounced decrease. The energy band gap and the refractive index are related to the threshold of absorption and transparency of the incident photons, respectively [47]. In a phase transition, a change of the refractive index occurs due to the modification of the physical properties. Even though the ZB and WZ structures have similar optical properties, the disorder at the critical point provokes a change in the degree of polarization, originating E_g and n to decrease [48, 49]. The thickness (τ) of the films was measured to be in the 210–250 nm range. In general, n follows a similar behavior to τ which is due to the direct relationship between both parameters in thin films [50]. In the vicinity of T_{bc}, a sharp decay in n is observed due to the disordered nature of these films. Vacancies and interstitial defects in the vicinity of T_b alter the average interplanar spacing among the different crystalline planes, causing a change in the porosity of the films and so the n [51].

In many cases, the photoluminescence (PL) spectrum of CdS thin films, containing native defects, are fitted with three main emissions: (i) upper near edge emission (*violet*) from surface states due to oxidation caused by the aqueous solutions [52–54], (ii) conduction band (CB) to interstitial Cd (I_{Cd}) (*green emission*), as aforementioned, undoped CdS prepared by chemical bath commonly contains an excess of Cd [44], even though, S and Cd vacancies (V) and I_S can also be present with lower density [44, 54, 55], and (iii) defect-to-defect transition emissions (*yellow* and *red*) [30, 56, 57]. PL

spectra, in the $1.3 \leq h\nu \leq 3.5$ eV range of CdS thin films, are displayed in Fig. 5a for all the films. For T_b's in the 90–97 °C interval (Fig. 5b), the PL spectra can be fitted using three bands: red emission in 1.83–1.90 eV (653—678 nm), green emission in 2.35–2.43 eV (510–528 nm), and blue violet band in 2.85–2.93 eV (423–435 nm). These spectra present a similar behavior except for $T_{bc} = 94$ °C. The PL intensity at this temperature is higher than other films and an additional emission peak (*blue*) emerges.

Figure 6a displays the main transitions within the forbidden band due to native defects in CdS, compiled from some reports [58–60], in particular, interstials (I) and vacancies (V) of Cd and S. The more probable radiative transitions which originate the PL bands of Fig. 5 are schematically depicted in Fig. 6a, where dotted lines represent emissions that are enhanced at $T_{bc} = 94$ °C. In Fig. 6a, emissions from the surface oxide to defects are not included. The difference of transitions from exciton level and CB are not appreciated at RT. The deconvolution of the three PL spectra for T_{bc} and those close to T_{bc} is depicted in Fig. 6b. The deconvolution-fitting spectra using Gaussian curves were performed to define the three bands aforementioned. However, for $T_{bc} = 94$ °C, the green band (~2.4 eV) splits into two bands. A new PL band appears at $h\nu = 2.53$ eV (blue). The authors of this work have associated this new band to the arising of interstitial Cd (I_{Cd}) donor defect, since a PL band at $h\nu \sim 2.25$ eV is associated to I_{Cd}'s in microcrystalline CdS, which splits into two levels under ZB-to-WZ phase transition [38, 39]. The presence was identified with I_{Cd}'s, which arise during the phase transition. The transition with band maximum at $h\nu \sim 2.25$ eV has been reported to be caused by I_{Cd}-to-V_{Cd} transitions [61, 62]. In the case of the CdS NP's, the emission has been shifted to 2.53 eV, i.e., from I_{Cd}'s to CB (light-blue dotted line in Fig. 6a). Observe that other transitions from I_{Cd}'s (green and yellow dotted lines) are also included as the FWHM of the light-blue band of Fig. 6b is very wide. During the phase transition, I_S and V_S are present, but in less proportion since I_{Cd}'s are produced
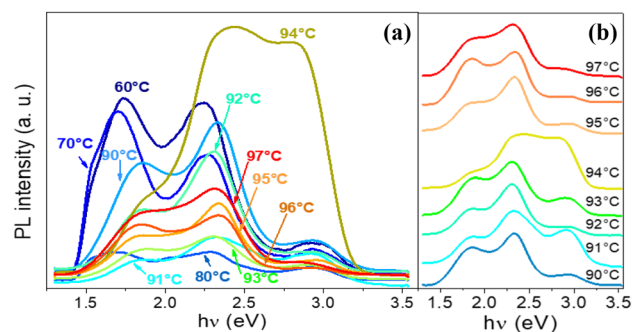

Fig. 5 PL spectra of the CdS films prepared at different T_b's (**a**) and for the films prepared at 90 °C $\leq T_b \leq$ 97 °C (**b**)

Fig. 6. **a** Electron transitions in CdS native defects, dashed emissions are enhanced only when $T_b = 94$ °C (defects indicate other defects like antisites, surface, etc.). **b** Deconvolution, using three or four Gaussian curves, of the PL spectra of the samples prepared with $T_b = 93$, 94 and 95 °C.
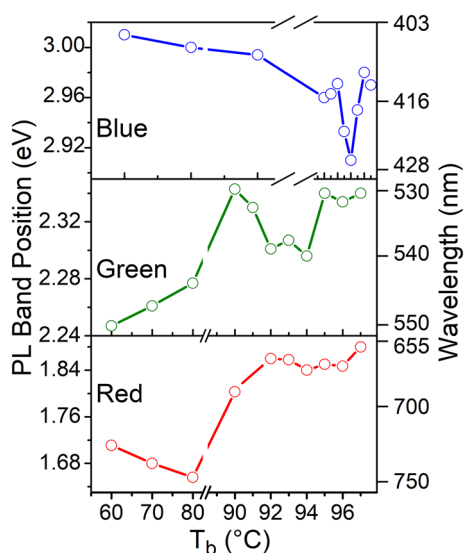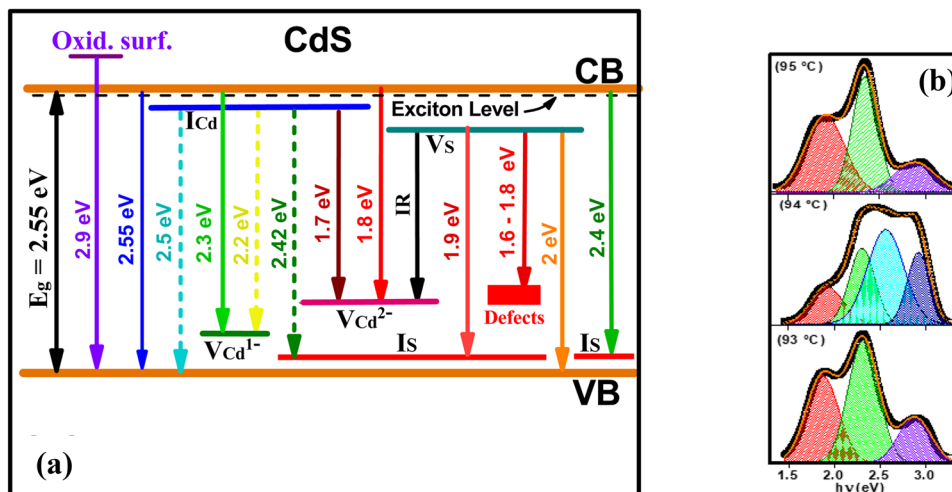

Fig. 7 Position of the blue, green, and red PL bands maximum obtained from the deconvolution of the spectra of all the samples

Fig. 8 PL in the high-energy region (2.7–3.7 eV) for the samples in the 91-96 °C range. The inset exhibits the absorbance of the sample grown at 95 °C in the 3.2–3.6 eV interval

in higher density because Cd^{2+} ions have lesser binding energy than S^{2-} ions [38, 63]. Moreover, Cd^{2+} ions have smaller ionic radius (109 pm) than S^{2-} (170 pm), which allows a higher mobility of Cd^{2+} and, consequently, generating a higher density of I_{Cd}'s and V_{Cd}'s. In this way, emissions from Cd defects were enhanced. Furthermore, it can be seen in Fig. 5a that the overall intensity of the PL bands for $T_b = 94$ °C is higher than those of the other samples due an increment of the defects density.

The position of the maxima of the three PL bands as a function of T_b is displayed in Fig. 7. The center of the blue band as a function of T_b is similar to the E_g *vs*. T_b behavior since E_g, donor, and acceptor levels depend on the size of NP's, which are subjected to internal stress from surface tension which, in turn, depends on the crystal size [64–66].
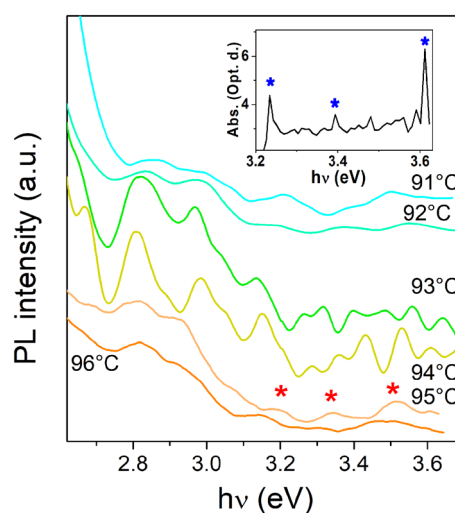
The green and red bands only show small depressions in the region close to T_{bc}.

Figure 8 shows the PL spectra in the region from 2.7 to 3.7 eV of the samples deposited at T_b from 91 to 96 °C. PL bands of this zone are radiative states located above the CB, which become accessible when the samples are excited with higher energy than the sample E_g [67, 68]. These signals are emitted with very small intensity, two orders of magnitude less than visible emissions, because most excited electrons decay rapidly to CB due to the phonons generation [68]. The discrete emissions have been also observed by Narasimman et al. in Zn-doped CdS, but the origin was not identified [69]. Notice in Fig. 8 that the three bands indicated in the bottom of the plot ($T_b = 95$ °C) by asterisks are also present in the spectra of samples of T_b equal to 91, 92, and 96 °C. These bands

split into two bands for T_b equals to 93 and 94 °C. This fact is the result that the high energy levels either split in two levels because of disorder, or the levels are at different energy in the ZB and WZ phases. The average value of the splitting energy in Fig. 8 is ∼0.07 eV, which is close to $\Delta E_g = E_{gWZ} - E_{gZB}$. Soltani et al. report [70] that $E_{gWZ} = 2.635$ eV, $E_{gZB} = 2.573$ eV, $\Delta E_g = 0.062$ eV, based on experimental measurements. The inset of Fig. 8 shows the absorption spectrum of the sample in the same energy region. Most of the absorbance spectra in that region are perturbed by noise; however, in some cases, some optical absorption peaks are observed, which could be related with these PL bands. These emissions seem to be the intra-atomic energy transitions of the Cd atom: (a) $5p^3P_0$, (b) $5p^3P_1$, and (c) $5p^3P_2$ to $5s^1S_0$, with energy transitions 3.74, 3.80, and 3.95 eV, respectively [71]; these values have an average value of 0.06 eV. Then, the emissions reported in this work come from Cd atoms transitions. This result suggests that the atomic orbitals of Cd are influenced by the internal crystal field of the corresponding lattice, due to different structural symmetry.

4 Conclusions

The influence of the ZB→WZ phase transformation on the optical properties of CdS thin films has been analyzed. The NP's CdS thin films were deposited on glass by chemical bath deposition, using microwaves in the temperature range of $60 \leq T_b \leq 97$ °C. The nanoparticulate CdS films grow in the cubic zinc blende crystalline phase for $60 \leq T_b < 94$ °C, in the hexagonal wurtzite structure for $94 < T_b \leq 97$ °C, and a mix of phases at the critical temperature ($T_{bc} = 94$ °C). The ZB→WZ transition occurs in the $93 < T_b < 95$ °C interval. The effect of the phase transformation on the optical properties is to displace the band gap to lower energies as the effect of the disorder, which in turn modifies the refractive index and PL emissions similarly. At the phase transition, the PL spectrum exhibits an additional band due to a high density of interstitials and vacancies of Cd, which arise due to the coexistence of both phases. High-energy emissions from the Cd atom intra-atomic transitions also show a split at the critical temperature.

References

1. B. Tell, Some optical properties of cadmium sulfide containing phosphorus and arsenic. J. Appl. Phys. **41**, 3789–3795 (1970)
2. H. Javed, F. Kalsoom, A. Zareen, N. Muhammad Arif, S. Muhammad, I. Azhar, Fluorescence modulation of cadmium sulfide quantum dots by azobenzene photochromic switch. Proc. R. Soc. A **472**, 692–712 (2016)
3. Y. Zhang, Q. Wang, The new progress of cadmium sulfide synthesis. Appl. Mech. Mater. **142**, 83–86 (2011)
4. H. Otsuka, Y. Nagasaki, K. Kataoka, Shell protected for biological and pharmaceutic applications. Adv. Drug Deliv. Rev. **5**, 403–419 (2003)
5. B. Ullrich, D.M. Bagnall, H. Sakai, Y. Segawa, photoluminescence and lasing of thin CdS films on glass formed by pulsed-laser-deposition. J, Lumin. **87–89**, 1162–1164 (2000)
6. R. Grover, R. Srivastava, O. Rana, A.K. Srivastava, K.K. Maurya, K.N. Sood, D.S. Mehta, M.N. Kamalasanan, Electroluminescence from hybrid organic–inorganic LEDs based on thermally evaporated CdS thin films. J. Lumin. **132**, 330–336 (2012)
7. P. Kumar, N. Saxena, F. Singh, V. Gupta, Ion beam assisted fortification of photoconduction and photosensitivity. Sens. Actuators A **279**, 343–350 (2018)
8. H. Li, X. Wang, J. Xu, Q. Zhang, Y. Bando, D. Golberg, Y. Ma, T. Zhai, One-dimensional CdS nanostructures: a promising candidate for optoelectronics. Adv. Mater. **25**, 3017–3037 (2013)
9. J.L. DiMeglio, A.G. Breuhaus-Alvarez, S. Li, B.M. Bartlett, Nitrate-mediated alcohol oxidation on cadmium sulfide photocatalysts. ACS Catal. **9**, 5732–5741 (2019)
10. E. Granot, F. Patolsky, I. Willner, Electrochemical assembly of a CdS semiconductor nanoparticle monolayer on surfaces: structural properties and photoelectrochemical applications. J. Phys. Chem. B **108**, 5875–5881 (2004)
11. C. Malarkodi, S. Rajeshkumar, K. Paulkumar, M. Vanaja, G. Gnanajobitha, G. Annadurai, Biosynthesis and antimicrobial activity of semiconductor nanoparticles against oral pathogens. Bioinorg. Chem. Appl. **2014**, 347167 (2014)
12. L. Saravanan, A. Pandurangan, R. Jayavel, Synthesis of cobalt-doped cadmium sulfide nanocrystals and their optical and magnetic properties. J. Nanopart. Res. **13**, 1621–1626 (2011)
13. Q. Wu, L. Huang, Z. Li, W. An, D. Liu, J. Lin, L. Tian, X. Wang, B. Liu, W. Qi, W. Wu, The potential application of raw cadmium sulfide nanoparticles as CT photographic developer. Nanoscale Res. Lett. **11**, 232–238 (2016)
14. N. Saxenaa, T. Kalsib, P. Uttamb, P. Kuma, Morphological evolution in nanocrystalline CdS thin films from flowers to salt rock-like structures. Opt. Mater. **84**, 625–630 (2018)
15. R. Banerjee, R. Jayakrishman, P. Ayyub, Effect of the size-induced structural transformation band gap in CdS nanoparticles. J. Phys. Condens. Matter **12**, 10647–10654 (2000)
16. J. Osugi, K. Shimizu, T. Nakamura, A. Onodera, Electrical conductivity of cadmium sulfide under high pressure and high temperature. J. Soc. Mater. Sci. Jpn. **17**, 47–51 (1968)
17. P. Cervantes, Q. Williams, Band structure of CdS and CdSe at high pressure. Phys. Rev. B **54**, 17585–17590 (1996)
18. M. Haase, A.P. Alivisatos, Arrested solid-solid phase transition in 4-nm-diameter CdS nanocrystals. J. Phys. Chem. **96**, 6756–6762 (1992)
19. W. Sun, J. Zhong, B. Zhang, K. Jiao, Application of cadmium sulfide nanoparticles as oligonucleotide labels for the electrochemical detection of NOS terminator gene sequences. Anal. Bioanal. Chem. **389**, 2179–2184 (2007)
20. S. Mukhopadhyay, I. Mondal, U. Pal, P.S. Devi, Fabrication of hierarchical ZnO/CdS heterostructured nanocomposites for enhanced hydrogen evolution from solar water splitting. Phys. Chem. Chem. Phys. **17**, 20407–20409 (2015)
21. Di Lang, G. Fan Liu, X.F. Qiu, Synthesis and visible-light photocatalytic performance of cadmium sulfide and oxide hexagonal nanoplates. ChemPlusChem **79**, 1726–1732 (2014)
22. Y.C. Cao, J. Wang, One-pot synthesis of high-quality zinc-blende CdS nanocrystals. J. Am. Chem. Soc. **126**, 14336–14337 (2004)
23. A.B. Bogoslovskaya, D.O. Grynko, E.G. Bortchagovsky, O.I. Gudymenko, Luminescent analysis of the quality of CdS

nanocrystals depending on technological parameters. SPQEO **22**, 231–236 (2019)

24. A. Gaiardo, B. Fabbri, V. Guidi, P. Bellutti, A. Giberti, S. Gherardi, L. Vanzetti, C. Malagù, G. Zonta, Metal sulfides as sensing materials for chemoresistive gas sensors. Sensors **16**, 296–319 (2016)

25. X. Li, C. Hu, Z. Zhao, K. Zhang, H. Liu, Three-dimensional CdS nanostructure for photoelectrochemical sensor. Sens. Actuator B Chem. **182**, 461–466 (2013)

26. F. Rodríguez-Mas, J.C. Ferrer, J.L. Alonso, S.F. de Ávila, Expanded electroluminescence in high load CdS nanocrystals PVK-based LEDs. Nanomaterials **9**, 1212–1219 (2019)

27. Y. Deng, J. Yang, R. Yang, K. Shen, D. Wang, D. Wang, Cu-doped CdS and its application in CdTe thin film solar cells. AIP Adv. **6**, 015203 (2016)

28. X. Yang, B. Wang, Mu Yu, M. Zheng, Y. Wang, Photocatalytic performance of cubic and hexagonal phase CdS synthesized via different Cd sources. J. Electron. Mater. **48**, 2895–2901 (2019)

29. S.-H. Wei, S.B. Zhang, Structure stability and carrier localization in CdX (X = S, Se, Te) semiconductors. Phys. Rev. B **62**, 6944–6947 (2000)

30. J. Marquez-Marín, C.G. Torres-Castanedo, G. Torres-Delgado, M.A. Aguilar-Frutis, R. Castanedo-Perez, O. Zelaya-Angel, Very sharp zinc blende-wurtzite phase transition of CdS. Superlattice Microstruct. **102**, 442–451 (2017)

31. A.A. Yadav, M.A. Barote, E.U. Masumdar, Studies on nanocrystalline cadmium sulphide (CdS) thin films deposited by spray pyrolysis. Sol. State Sci. **12**, 1173–1177 (2010)

32. G.L. Stansfield, P.V. Vanitha, H.M. Johnston, D. Fan, H. Alqahtani, L. Hague, M. Grell, D.P. JohnThomas, Growth of nanocrystals and thin films at the water–oil interface. Phil. Trans. R. Soc. A **368**, 4313–4330 (2010)

33. V. Gevorgyan, L.A. Hakhoyan, N. Mangasaryan, P.P. Gladyshev, Substrate temperature and annealing effects on the structural and optical properties of nano-CdS films deposited by vacuum flash evaporation technique. Chalcog. Lett. **13**, 331–338 (2016)

34. L.G. Daza, R. Castro-Rodríguez, M. Cirerol-Carrillo, E.A. Martín-Tovar, J. Méndez-Gamboa, R. Medina-Esquivel, I. Pérez-Quintana, A. Iribarren, Nanocolumnar CdS thin films grown by glancing angle deposition from a sublimate vapor effusion source. J. Appl. Res. Technol. **15**, 271–277 (2017)

35. C.C. Yang, S. Li, Size, dimensionality, and constituent stoichiometry dependence of bandgap energies in semiconductor quantum dots and wires. J. Phys. Chem. C **112**, 2851–2856 (2008)

36. S.R. Stebbing, R.W. Hughes, P.A. Reynolds, Sizing, stoichiometry and optical absorbance variations of colloidal cadmium sulphide nanoparticles. Adv. Colloids Interface Sci. **147–148**, 272–280 (2009)

37. S. Takeuchi, K. Suzuki, K. Maeda, H. Iwanaga, Staking-fault energy of II–VI compounds. Philos. Mag. **30**, 171–178 (1984)

38. R. Lozada-Morales, O. Zelaya-Angel, G. Torres-Delgado, On the yellow-band emission in CdS films. Appl. Phys. A **73**, 61–65 (2001)

39. R. Lozada-Moralesa, O. Zelaya-Angelb, G. Torres-Delgado, Photoluminescence in cubic and hexagonal CdS films. Appl. Surf. Sci. **175–176**, 562–566 (2001)

40. H. Moualkia, S. Hariech, M.S. Aida, Structural and optical properties of CdS thin films grown by chemical bath deposition. Thin Solid Films **518**, 1259–1262 (2009)

41. Z. Zhou, M. Li, P. Wu, L. Guo, Revisiting the zinc-blende/wurtzite heterocrystalline structure in CdS. Adv. Condens. Matter Phys. **2014**, 361328 (2014)

42. R. Raj, A. Hoda, N. Kumari, B.C. Rai, Quantum confinement in cadmium sulfide semiconductor. Int. J. Adv. Res. Eng. Technol. **9**, 1–9 (2018)

43. U.S. Patle, Photoluminescence studies of nanocrystalline films of cadmium sulphide. Int. J. Nanotechnol. Appl. **11**, 9–15 (2017)

44. J.A. Dávila-Pintle, R. Lozada-Morales, M.R. Palomino-Merino, J.A. Rivera-Márquez, O.P. Moreno, O. Zelaya-Angel, Electrical properties of Er-doped CdS thin films. J. Appl. Phys. **101**, 013712–13715 (2007)

45. J.O. Winter, N. Gomez, S. Gatzert, C.E. Schmidt, B.A. Korgela, Variation of cadmium sulfide nanoparticle size and photoluminescence intensity with altered aqueous synthesis conditions. Colloids Surf. A **254**, 147–157 (2005)

46. M. Reddy, N.V. Prasad, Properties of CdS chemically deposited thin films on the effect of ammonia concentration. IOSR J. Appl. Phys. **4**, 01–07 (2013)

47. S.K. Tripathy, Refractive indices of semiconductors from energy gaps. Opt. Mater. **46**, 240–246 (2015)

48. A. Dejneka, I. Aulika, V. Trepakov, J. Krepelka, L. Jastrabik, Z. Hubicka, A. Lynnyk, Spectroscopic ellipsometry applied to phase transitions in solids: possibilities and limitations. Opt. Exp. **17**, 14322–14338 (2009)

49. K. Sokolowski-Tinten, J. Bialkowski, D. von der Linde, Ultrafast laser-induced order-disorder transitions in semiconductors. Phys. Rev. B **51**, 14186–14198 (1995)

50. Y. Akaltun, M.A. Yıldırım, A. Ateş, M. Yıldırımc, The relationship between refractive index-energy gap and the film thickness effect on the characteristic parameters of CdSe thin films. Opt. Commun. **284**, 2307–2311 (2011)

51. L. González-García, G. Lozano, A. Barranco, H. Míguez, A.R. González-Elipe, TiO2–SiO2 one-dimensional photonic crystals of controlled porosity by glancing angle physical vapour deposition. J. Mater. Chem. **20**, 6408–6412 (2010)

52. W. Lee, H. Kim, D.-R. Jung, J. Kim, C. Nahm, J. Lee, S. Kang, B. Lee, B. Park, An effective oxidation approach for luminescence enhancement in CdS quantum dots by H2O2. Nanoscale Res. Lett. **7**, 672–675 (2012)

53. H.L. Pushpalatha, R. Ganesha, X-ray photoelectron spectroscopic studies of CdS semiconductor thin films deposited by photochemical deposition. Int. J. Chem. Technol. Res. **7**, 2171–2175 (2014)

54. V.D. Moreno-Regino, C.G. Torres-Castanedo, J.S. Arias-Ceron, M.A. Badillo-Avila, J. Marquez-Marín, R. Castanedo-Perez, O. Zelaya-Angel, G. Torres-Delgado, Effect of the thiourea incorporation velocity and RTA post-deposit treatments, on the properties of CdS films deposited by chemical bath deposition. J. Alloys Compd. **803**, 1168–1177 (2019)

55. W.-D. Park, Photoluminescence of nanocrystalline CdS thin films prepared by chemical bath deposition. Electr. Electron. Mater. **11**, 170–173 (2010)

56. A. Srivastava, H.L. Vishwakarma, Photoluminescence of chemically synthesized CdS nanoparticles. Int. J. Pure Appl. Phys. **6**, 347–351 (2010)

57. S.K. Mishra, R.K. Srivastava, S.G. Prakash, R.S. Yadav, A.C. Panday, Structural, photoconductivity and photoluminescence characterization of cadmium sulfide quantum dots prepared by a co-precipitation method. Electron. Mater. Lett. **7**, 31 (2011)

58. S. Singh, S. Garg, J. Chahal, K. Raheja, D. Singh, M.L. Singla, Luminescent behavior of cadmium sulfide quantum dots for gallic acid estimation. Nanotechnology **24**, 115602–115608 (2013)

59. T. Gutu, D.K. Gale, C. Jeffryes, W. Wang, C.-H. Chang, G.L. Rorrer, J. Jiao, Electron microscopy and optical characterization of cadmium sulphide nanocrystals deposited on the patterned surface of diatom biosilica. J. Nanomater. **2009**, 860536 (2009)

60. S.R. Meher, D.K. Kaushik, A. Subrahmanyam, Native defects in sol–gel derived CdS buffer layers for photovoltaic applications. J. Mater. Sci. Mater. Electron. **28**, 6033–6046 (2017)

61. A.G. Stanley, *Cadmium Sulfide* (Jet Propulsion Laboratory Pub., Pasadena, 1978), pp. 41–63

62. A.E. Abken, D.P. Halliday, K. Durose, Photoluminescence study of polycrystalline photovoltaic CdS thin film layers grown by close-spaced sublimation and chemical bath deposition. J. Appl. Phys. **105**, 064515–64519 (2009)

63. I.K. Battisha, H.H. Afify, G. Abd El Fattah, Y. Badr, Raman and photoluminescence studies of pure and Sn-enriched thin films of CdS prepared by spray pyrolysis. Fizika A **11**, 31–42 (2002)

64. S. Cuenot, C. Frétigny, S. Demoustier-Champagne, B. Nysten, Surface tension effect on the mechanical properties of nanomaterials measured by atomic force microscopy. Phys. Rev. B **69**, 165410–165510 (2004)

65. T. Ba Hoang, L.V. Titova, H.E. Jackson, L.M. Smith, J.M. Yarrison-Rice, Temperature dependent photoluminescence of single CdS nanowires. Appl. Phys. Lett. **89**, 123123 (2006)

66. R. Lozada-Morales, O.P. Moreno, S.A. Tomás, O. Zelaya-Angel, Influence of internal stress on the optical properties of CdS: Cu nanoparticles. Opt. Mater. **35**, 1023–1028 (2013)

67. M. Maleki, M.S. Ghamsari, Sh Mirdamadi, R. Ghasemzadeh, A facile route for preparation of CdS nanoparticles. Semicond. Phys. Quant. Electron. Optoelectr. **10**, 30–32 (2007)

68. V.N. Pak, S.M. Shilov, Y. Yu Gavronskaya, Dependence of cadmium sulfide fluorescence on the excitation light energy. Arch. Org. Inorg. Chem. Sci. **1**, 97–99 (2018)

69. V. Narasimman, V.S. Nagarethinam, K. Usharani, A.R. Balu, Structural, morphological, optical and electrical properties of spray deposited ternary CdZns thin films. Int. J. Thin. Film Sci. Technol. **5**, 17–24 (2016)

70. N. Soltani, E. Gharibshahi, E. Saion, Band gap of cubic and hexagonal CdS quantum dots—experimental and theoretical studies. Chalcog. Lett. **9**, 321–328 (2012)

71. G.M. Petrov, T.S. Petrova, A. Ogoyski, A.B. Blagoev, Cd–Ne direct current glow discharge: an efficient source of ultraviolet radiation. Appl. Phys. Lett. **77**, 40–42 (2000)